Time-Resolved Fluorescence Anisotropy as a Tool to Study Guest–Cucurbit[n]uril–Protein Ternary Supramolecular Interactions

ARTICLE *in* PHOTOCHEMICAL AND PHOTOBIOLOGICAL SCIENCES · FEBRUARY 2015

Impact Factor: 2.27 · DOI: 10.1039/C4PP00479E

4 AUTHORS, INCLUDING:

Denis Fuentealba

Pontifical Catholic University of Chile

13 PUBLICATIONS **132** CITATIONS

SEE PROFILE

Photochemical & Photobiological Sciences

PAPER

View Article Online
View Journal

Cite this: DOI: 10.1039/c4pp00479e

Time-resolved fluorescence anisotropy as a tool to study guest–cucurbit[*n*]uril–protein ternary supramolecular interactions†

Karina Scholtbach,[a] Ítalo Venegas,[a] Cornelia Bohne[b] and Denis Fuentealba*[a]

Ternary supramolecular complexes involving cucurbit[*n*]urils and proteins are of potential interest for improving drug transport and delivery. We report here time-resolved fluorescence studies for acridine orange complexes with cucurbit[7]uril and cucurbit[8]uril in the presence of human serum albumin as a model system. A detailed characterization of the fluorescence lifetime and anisotropy properties of the different acridine orange complexes with cucurbit[*n*]urils and human serum albumin was performed. Of particular importance is the analysis of the stepwise binding for acridine orange–cucurbit[8]uril complexes and the assignment of the fluorescence and anisotropy properties to the 2 : 1 complex. Anisotropy decay measurements were essential to detect protein-bound species and to discriminate between different complexes. Based on the fluorescence evidence, ternary interactions with the protein are suggested for the acridine orange–cucurbit[7]uril complex but not for the cucurbit[8]uril complex. We highlight here the usability and sensitivity of the combined fluorescence analysis.

Received 16th December 2014,
Accepted 22nd January 2015

DOI: 10.1039/c4pp00479e

www.rsc.org/pps

1. Introduction

Research involving cucurbit[*n*]urils (CB[*n*], *n* = 5–10, Scheme 1) has been increasingly important during the last decade due to their binding and recognition properties.[1–3] These macrocycles are composed of several glycoluril units joined by methylene groups in a cyclic manner, and their cavity sizes range from 82 Å^3 to 870 Å^3.[1–3]

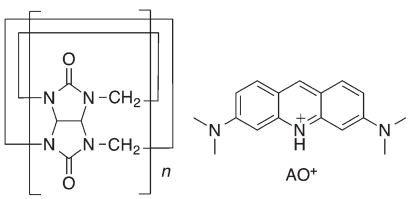

Scheme 1 Cucurbit[*n*]uril (CB[*n*], *n* = 7 or 8) and acridine orange (AO^+) structures.

Some of the latest studies involving CB[*n*] include the recognition and sensing of biomolecules,[4,5] a supramolecular velcro,[6] hybrid colloids[7] and tissue engineering.[8] A particular area that has taken advantage of CB[*n*] properties is drug delivery.[9–14] The capacity of CB[*n*] to encapsulate and stabilize several drugs,[11] cross the cell membrane,[15] and their low toxicity,[16,17] are very suitable for this kind of application.[12] In this context, the use of supramolecular systems such as CB[*n*] to improve the bioavailability of drugs and control their release is likely to play an important role in the further development of drug delivery systems.[14]

Unwanted interactions between guest–CB[*n*] complexes and proteins in biological media to form guest–CB[*n*]–protein ternary complexes‡ could have unexpected effects for drug delivery applications. In this sense, photoactive drugs are a particularly important example of such effects since protein binding can modify their photoactivity,[18] and in turn the photophysical properties of the drug can be used to probe this supramolecular environment.[19] When considering that photoactive drugs can also bind to CB[*n*],[20–22] a variety of supramolecular interactions can be present in the system and several techniques can be used to assess them.[23] Guest–CB[*n*] complexes are dynamic, a factor that is particularly important when considering self-sorting between different complexes. Although some guest–CB[*n*] complexes are

[a]*Laboratorio de Química Biológica, Departamento de Química Física, Facultad de Química, Pontificia Universidad Católica de Chile, Santiago, Chile.*
E-mail: dlfuente@uc.cl
[b]*Department of Chemistry, University of Victoria, P.O. Box 3065, Victoria, BC, Canada V8W 3V6*

† Electronic supplementary information (ESI) available: Numerical analysis, Trp-Gly-Gly/CB[8] binding isotherms, static and dynamic quenching studies and the correction procedure, AO^+/HSA binding, anisotropy decays for CB[8] samples and simulations. See DOI: 10.1039/c4pp00479e

‡ Note that in this work the term "ternary complex" refers to the guest–CB[*n*]–protein ternary complex and must not be confused with CB[8] 1 : 1 : 1 or 2 : 1 complexes.

amenable to be studied on NMR time-scales,[24,25] other complexes have much faster dynamics.[26–28]

A simple yet powerful tool to study these systems is fluorescence spectroscopy, which is both sensitive and occurs on a fast time-scale, so that guest relocation from CB[*n*] does not happen within the time-frame of the measurement.[23]

When the guest has observable photophysical properties, such as changes in fluorescence emission, the identification of supramolecular assemblies depends almost exclusively on the differential emission properties of free guest and the guest–CB[*n*]–protein ternary complex. Previous studies have shown that large fluorescence changes for triphenylmethane dye *brilliant green* appear upon ternary complex formation with CB[7] and bovine serum albumin (BSA).[29] On the other hand, for the dye tetra(1-methylpyridinium)porphyrin in the presence of CB[8], the formation of a ternary complex is evident by the quenching of the tryptophan emission in BSA.[22] Such evident changes in the photophysical properties of the complex might not be ubiquitous and the absence of such changes cannot be taken as proof for the non-existence of the ternary complex.

In this context, we have shown before that time-resolved fluorescence anisotropy is a remarkable tool to analyze multiple protein-bound species even when they have the same fluorescence lifetimes.[30] Therefore, in this work we evaluated the usability of time-resolved fluorescence anisotropy in the detection of guest–CB[*n*]–protein ternary interactions. We chose to study such interactions in a model system (Scheme 1) composed of CB[7] or CB[8]: the photoactive drug acridine orange (AO^+) and human serum albumin (HSA). AO^+ was chosen because the formation of inclusion complexes with both CB[7] and CB[8],[20,21] and with another albumin[31] has been well documented. HSA fluorescence quenching suggested the formation of a AO^+@CB[7] : HSA ternary complex, while the $(AO^+)_2$@CB[8] complex did not interact with HSA. Quenching constants and fluorescence lifetimes for the AO^+@CB[7] : HSA ternary complex were undistinguishable from AO^+@CB[7] or AO^+ : HSA complexes. Nonetheless, anisotropy measurements were very sensitive to the formation of protein-bound species and allowed a clear discrimination between multiple free and complexed species.

2. Experimental

2.1. Chemicals

Acridine orange hydrochloride (AO^+, 99%), human serum albumin (HSA, essentially globulin free, ≥99%), bis(cyclopentadienyl)cobalt(III) hexafluorophosphate (Cob^+, 98%), cucurbit[7]uril (CB[7]) and cucurbit[8]uril (CB[8]) were obtained from Sigma and were used without further purification. Sodium dihydrogen phosphate monohydrate (99%) and sodium hydrogen phosphate anhydrous (≥99%) were purchased from Merck. L-Tryptophanylglycylglycine (Trp-Gly-Gly, ≥99%) was purchased from Chem-Impex International and its purity was confirmed by ^{1}H NMR. Ultrapure water from a Sybron Barnstead Nanopure or a Milli-Q water purifying system was used to prepare all the solutions (resistivity ≥17.8 MΩ cm).

2.2. Solution preparation

Stock solutions of AO^+ were prepared in water (~1 mM) and their concentrations were assessed using its molar extinction coefficient (AO^+, $\varepsilon_{491} = 6.2 \times 10^4$ M^{-1} cm^{-1}).[32] Stock solutions of CB[7] (~1 mM) were prepared in water, while those of CB[8] (~50 μM) were prepared in 10 mM phosphate buffer pH 7.0 with the aid of sonication and vigorous shaking. CB[8] stock solutions were filtered through a 0.2 μm syringe filter after the preparation to remove any undissolved solids. CB[7] and CB[8] stock solutions were titrated against a known concentration of Cob^+ (3–15 μM) determined using its molar extinction coefficient ($\varepsilon_{261} = 3.42 \times 10^4$ M^{-1} cm^{-1}).[33] Concentrated phosphate buffer solutions (0.1 M pH 7.0) were prepared by dissolving 0.4614 g of anhydrous Na_2HPO_4 and 0.2415 g of $NaH_2PO_4 \times H_2O$ in water in a 50.00 mL volumetric flask. The pH of the buffer was checked with a pHmeter (Hanna HI2221) to be 7.00 ± 0.03. All samples for measurements were prepared by diluting stock solutions. For binding constant determinations, 10–15 samples were prepared by mixing different proportions of a solution containing only AO^+ with a solution containing both AO^+ and the highest concentration of CB[*n*], thus ensuring that the concentration of AO^+ in all the solutions was the same. The samples were shaken for one hour at 20 °C using a Hilab thermoshaker. All the experiments were carried out in 10 mM phosphate buffer pH 7.0 containing a concentration of sodium ions of 16.5 mM.

2.3. Absorption and fluorescence spectra

Absorption spectra were recorded using a Cary 1 spectrophotometer at room temperature and they were corrected for the absorption of a control solution containing the buffer. Some measurements were performed using an HP8453 spectrophotometer. Steady-state fluorescence spectra were recorded using a LS55 PerkinElmer fluorescence spectrometer at 20.0 ± 0.1 °C. The bandwidth used for the excitation monochromator was 2.5 nm and the emission bandwidth was either 2.5 nm or 5 nm. Fluorescence spectra were corrected for the emission of the control solution containing the buffer, which accounted for the Raman emission of the solvent.

2.4. Determination of binding constants

The fluorescence data for the determination of the binding constants for AO^+ and CB[7] were collected by exciting the samples at 370 nm, where the change in the absorption of the samples at increasing concentrations of CB[7] was negligible (absorbance change ≤0.001 in the presence of CB[7]). The emission intensities were collected at 509 nm. In the case of AO^+ and CB[8], the samples were excited at 480 nm at the isosbestic point. In this case, the emission intensities were measured at 523 nm. The data for the dependence of the changes in the fluorescence intensity with the concentration of CB[*n*]s were fit using numerical analysis by solving a set of equations involving the chemical equilibria and mass balances of the species involved (see the ESI† for details). The experiments were repeated at least three times and the errors pre-

sented correspond to standard deviations from independent experiments.

2.5. HSA fluorescence quenching

HSA fluorescence quenching data by addition of AO^+ in the presence of CB[7] were collected by exciting the samples at 280 nm and measuring the emission at 340 nm. AO^+ absorbs at excitation and emission wavelengths, and the emission intensities were corrected for the inner-filter effect,[34,35] caused by the competitive absorption of photons by HSA and AO^+ (see the ESI† for details). The fluorescence quenching data were analyzed according to the Stern–Volmer plot (eqn (1)), where I_0 corresponds to the fluorescence intensity in the absence of the quencher (Q), I corresponds to the fluorescence intensity in the presence of different concentrations of the quencher and K_{SV} corresponds to the Stern–Volmer constant.[34] If the quenching is static, the Stern–Volmer constant corresponds to a binding constant.[34]

$$\frac{I_0}{I} = 1 + K_{SV}[Q] \quad (1)$$

2.6. Time-resolved fluorescence and anisotropy measurements

Fluorescence and anisotropy decays were measured using an OB920 single photon counting system from Edinburgh Instruments. The excitation source for AO^+ was a 404 nm picosecond laser diode (EPL-405, bandwidth of 7 nm) working with a repetition rate of 1 MHz to 10 MHz. The detector was a MCP-PMT from Hamamatsu with a response time <25 ps. For the fluorescence of HSA, a 278 nm light-emitting diode was used (EPLD-280, bandwidth of 10 nm) working with a repetition rate of 10 MHz.

The light emitted by the 404 nm laser diode was vertically polarized. Therefore, the emission was collected through a polarizer/monochromator set (16 nm bandwidth) at the magic angle (54.7°) to eliminate any polarization effect when determining fluorescence lifetimes. For the 278 nm light-emitting diode, the emission polarizer was not in place when collecting the emission because the light was not polarized. The maximum number of counts collected to determine fluorescence lifetimes was 2000 or 10 000 counts. The emission was collected at the maxima for each species. The instrument response function (IRF) was obtained by scattering the excitation light using a diluted Ludox solution. The IRF was reconvoluted with the fluorescence decays in order to obtain fluorescence lifetimes. The fluorescence decays were fit using eqn (2), where the pre-exponential factor A_i is related to the contribution of one species to the intensity of the decay and τ_i corresponds to the fluorescence lifetime of different species. The goodness of the fit was assessed by the observation of randomly distributed residuals around zero and a χ^2 value between 0.9 and 1.2.[36]

$$I(t) = I_0 \sum_1^i A_i e^{-t/\tau_i} \quad (2)$$

Polarized fluorescence decays were collected at the vertical (I_{VV}) and horizontal (I_{VH}) positions of the emission polarizer. Both decays were collected in the same conditions and for the same amount of time, in order to reach about 10 000 counts for the channel with a maximum intensity (which corresponded to I_{VV}). A high number of counts were necessary to increase the signal-to-noise ratio for anisotropy decays. The anisotropy decay was calculated according to eqn (3).

$$r(t) = \frac{I_{VV}(t) - GI_{VH}(t)}{I_{VV}(t) + 2GI_{VH}(t)} \quad (3)$$

G corresponds to a correction factor for the sensitivity of the optics to light with different polarizations. The G factor was recovered using the FAST software (Edinburgh Instruments) for the samples in the absence of HSA, for which the rotational correlation time was short and the anisotropy decayed to zero within the time scale for the measurement.[30] This procedure is essential since small changes in the G factor can bring about changes in the baseline for the anisotropy of the samples. The G factor determined in the absence of HSA was then used for anisotropy decays in the presence of HSA.

2.7. Analysis of the anisotropy decays

The anisotropy decay of a complex system containing more than one type of fluorophore is related to both the number of different species, *e.g.* fluorophores in water and in different complexes, and the lifetimes of each species. In the simplest case where there is one emissive species, one lifetime and the shape of the molecule is close to a sphere, the decay is mono-exponential (eqn (4), $j = 1$, $\beta = 1$). The fundamental anisotropy r_0 is an intrinsic property of the molecule with values between −0.2 and 0.4 and which depends on the excitation wavelength.[34] The r_0 value is measured in a high viscosity medium where the fluorophore does not rotate while excited. In the case of fluorophores that have the same excited state lifetimes but are in environments where they rotate at different speeds, the decay is fit to a sum of exponentials (eqn (4), $j > 1$). This analysis also assumes that the rotors are spherical. Each species has a different rotational correlation time (ϕ_j), and the pre-exponential factor β_j corresponds to the contribution of each species to the intensity of the anisotropy decay.

$$r(t) = r_0 \sum_1^j \beta_j e^{-t/\phi_j} \quad (4)$$

The anisotropy decay for the case where each fluorescent species has a different lifetime and a different rotational correlation time is analyzed using the associated model (eqn (5)), which assumes that the species do not interconvert during the fluorescence decay measurement.[37] This assumption is reasonable in this work since the dynamics of guest–CB[n] binding was shown to occur on time scales much longer[26] than the tenth of nanosecond time scale for the anisotropy decay of AO^+ (see below). The key difference when species with more than one lifetime are present is that $r(t)$ is a function of the fractional intensity (f_i, eqn (6)) for each species, where f_i is deter-

mined by the pre-exponential factor and lifetimes measured when no polarization effects are present, *i.e.* at the magic angle for the emission polarizer (54.7°).

$$r(t) = \sum_{1}^{i} f_i(t) r_i(t) \quad (5)$$

$$f_i(t) = \frac{A_i e^{-t/\tau_i}}{\sum_{1}^{i} A_i e^{-t/\tau_i}} \quad (6)$$

3. Results

Before analyzing the interaction of AO^+@CB[n] complexes with HSA, it was necessary to first establish the fluorescence properties of AO^+ free in water and bound to CB[7], CB[8] or HSA. It must be noted that some of these properties were compared with already reported data in the literature, while others are reported for the first time in this work, as mentioned below.

3.1. Absorption and fluorescence spectra for AO^+ complexes with CB[n]

Complexation of AO^+ can be readily observed by absorption and fluorescence spectroscopy (Fig. 1) and a different behavior was observed when AO^+ was bound to CB[7] or CB[8], as reported in the literature.[15,20,21] The maxima for the monoprotonated AO^+ (pK_a of 10)[21,38] in 10 mM phosphate buffer at pH 7.0 were found at 492 nm for absorption and at 525 nm for emission, in good agreement with the literature.[21,39] In the presence of CB[7] both the absorption and emission maxima were blue-shifted to 485 nm and 508 nm, respectively.[20,21] In the presence of CB[8] the absorption maximum was blue-shifted to 468 nm while the emission maximum was red-shifted to 560 nm.[15,20] Of importance to this work is that the fluorescence intensity increases noticeably in the presence of CB[7], while in the presence of CB[8] the fluorescence intensity decreases considerably (Fig. 1, inset). AO^+ can form dimers in aqueous solution at high concentrations (K = 2200 M^{-1}).[20,39] Under our experimental conditions in the absence of CB[n] (AO^+ 2–3 μM), the monomeric AO^+ accounted for 99% of the species present. Therefore the changes in the absorption and emission spectra are not due to a shift in the monomer–dimer equilibrium.

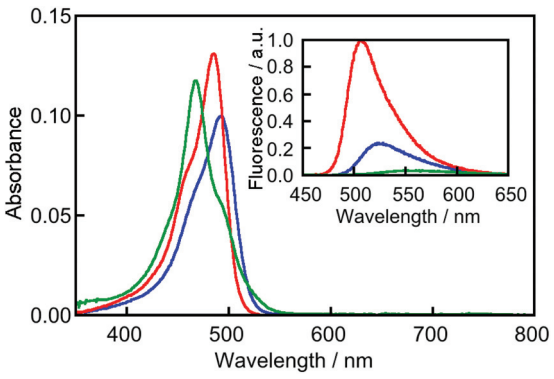

Fig. 1 Absorption spectra for AO^+ (2 μM) in the absence (blue) and presence of 50 μM CB[7] (red) or 20 μM CB[8] (green) in 10 mM phosphate buffer pH 7.0 at 20 °C. Inset: fluorescence spectra for the same samples.

3.2. Binding isotherms for AO^+ complexes with CB[n] and HSA

Determination of binding constants for AO^+@CB[n] complexes is essential to determine the species of AO^+ present at different experimental conditions. Binding constants for CB[n] complexes found in the literature are determined with different techniques (*e.g.* absorption, fluorescence, NMR, ITC) and are affected by conditions such as solvent, pH and temperature. In particular cations, such as sodium and hydronium, bind to CB[n] decreasing their effective concentrations leading to changes in the overall binding constant of guests.[26] In this work, we used a constant concentration of Na^+ (16.5 mM) given by a 10 mM phosphate buffer at pH 7.0. Therefore, the determined binding constants correspond to overall equilibrium constants that are conditional to the given Na^+ concentration.

The binding constant for AO^+ with CB[7] of (3 ± 1) × 10^6 M^{-1} was determined by fluorescence measurements (Fig. 2, inset) using numerical analysis as described previously[26] (see the ESI† for details). Other reported binding constants are 2 × 10^5 M^{-1} in water adjusted to pH 7,[21] 3.07 × 10^6 M^{-1} in water adjusted to pH 5.5[20] and 8.7 × 10^5 M^{-1} in phosphate buffered saline (PBS).[15] The binding constant determined in this work is within the range of values reported in the literature and the differences observed are likely due to the use of different experimental conditions as mentioned before.

CB[8] forms 1 : 1 and 2 : 1 complexes with AO^+, and therefore, the equilibrium involves two steps for the binding of the

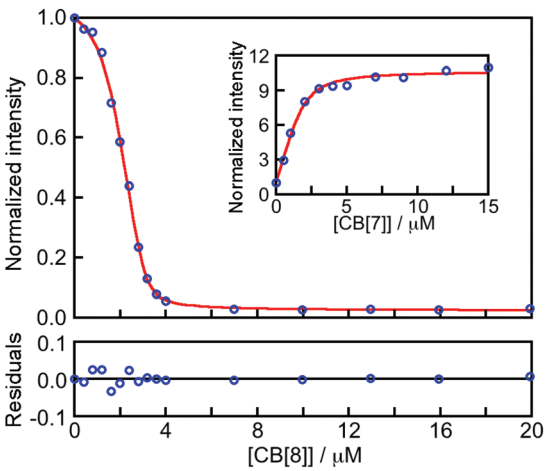

Fig. 2 Fluorescence intensity for a 3 μM AO^+ solution in the presence of different concentrations of CB[8]. Inset: fluorescence intensity for a 2 μM AO^+ solution in the presence of different concentrations of CB[7]. All samples in 10 mM phosphate buffer pH 7.0 at 20 °C. The data were fit to eqn (S1)–(S4) for CB[7] and S5–S9 for CB[8] as described in the ESI.†

Table 1 Fluorescence lifetimes and rotational correlation times for different AO^+ species in 10 mM phosphate buffer pH 7.0 at 20 °C

Samples (ratio)	τ_1/ns (A_1)	τ_2/ns (A_2)	ϕ_1/ns (β_1)	ϕ_2/ns (β_2)	r_0
AO^+	2.01 ± 0.04 (1)	—	0.12 ± 0.01 (1)	—	0.30 ± 0.09
AO^+ + CB[7] (1 : 25)	3.46 ± 0.02 (1)	—	0.39 ± 0.01 (1)	—	0.32 ± 0.01
AO^+ + CB[8] (1 : 10)	2.0^{fixed} (0.06 ± 0.01)	6.87 ± 0.02 (0.94 ± 0.01)	$0.12^{fixed a}$	0.63 ± 0.03^a	0.28 ± 0.01
AO^+ + HSA (1 : 5)	1.98 ± 0.02 (0.96 ± 0.01)	4.77 ± 0.01 (0.04 ± 0.01)	0.15 ± 0.07^a	$55^{fixed\ a}$	0.30 ± 0.01

[a] The anisotropy decay was fit using eqn (4)–(6) ($i = 2, j = 2$).

first and second AO^+ molecules. This fact implies that the numerical fit includes two overall equilibrium constants and two emission efficiencies. Preliminary analysis showed that the emission efficiency for the 2 : 1 complex could not be recovered from the fit. Thus, this parameter was independently determined from the fluorescence intensity of a sample containing a 5-fold excess of AO^+ over CB[8], where the main species is the 2 : 1 complex and the 1 : 1 complex is negligible.

The stepwise binding constants determined from the fit of the binding isotherm (Fig. 2) were $(2.5 \pm 0.4) \times 10^8$ M^{-1} and $(1.7 \pm 0.3) \times 10^6$ M^{-1} for the first and second AO^+ molecules bound to CB[8]. These stepwise binding constants have not been reported before, however the overall binding of the two AO^+ obtained here of $(4 \pm 1) \times 10^{14}$ M^{-2} is within the range reported previously of 2.27×10^{16} M^{-2} in water (pH 5.5)[20] and 5.2×10^{13} M^{-2} in PBS.[15] The obtained stepwise binding constants for AO^+ with CB[8] differ by a factor of 150 from each other, which is much larger than the theoretical factor of 4 expected for the binding of a guest to a host with two independent binding sites.[40] Any difference much larger than 4, as observed for AO^+ bound to CB[8], indicates a negative cooperativity for the two binding events. In order to corroborate our analysis, we determined the stepwise binding constants for a known system, *i.e.* the inclusion of tryptophanylglycylglycine into CB[8], for which the ratio between the stepwise binding constants was reported to be 4.6 using ITC.[41] We determined a ratio of 4.7 for this tripeptide using fluorescence data and numerical analysis, which is in very good agreement with the reported value (see Fig. S1 in the ESI†). The reason for the large negative cooperativity observed for the binding of two AO^+ molecules to CB[8] compared to the tripeptide is likely to be related to the electrostatic repulsion between the central positive charges in AO^+ molecules, meanwhile for the tripeptide the charge is localized on the terminal amino group.

Another important species to be considered when analyzing ternary interactions with the protein is the formation of a AO^+ : HSA complex. We determined the binding of AO^+ to HSA using the quenching of the fluorescence of the tryptophan residue in the protein, as previously reported for BSA.[31] The binding constant obtained from Stern–Volmer quenching plots (see Fig. S2 in the ESI†) is $(2.5 \pm 0.4) \times 10^4$ M^{-1}. Binding constants obtained from quenching measurements require a binding site for AO^+ close to the tryptophan residue,[22,31] which has been described as Sudlow's site I.[42] If binding to other sites occurs, this value could possibly be underestimated. Therefore, we also determined the binding constant for AO^+ with HSA from a binding isotherm using the changes in the AO^+ fluorescence intensity in a similar manner to the determination of the binding of AO^+ to CB[*n*] shown above (see Fig. S3 in the ESI†). We obtained the value of $(2.0 \pm 0.5) \times 10^5$ M^{-1}, which suggests that AO^+ can bind to other sites in HSA far from the tryptophan residue. It must be noted that the association efficiency of AO^+ with HSA is between 15 and 120 times lower than the AO^+ complexation with CB[7] and more than 1000 times lower than that with CB[8]. This is an important information because if the binding constant for AO^+ with HSA was higher than with CB[*n*]s, displacement would occur from the CB[*n*]s into HSA and no ternary complex would be formed.[43]

3.3. Fluorescence lifetimes and rotational correlation times for AO^+ complexes with CB[*n*]

The fluorescence decays were monoexponential for AO^+ in the absence and presence of excess CB[7], indicating the presence of a single species in each case (see Fig. S4 in the ESI†). These species with fluorescence lifetimes of 2.01 ± 0.04 ns and 3.46 ± 0.02 ns correspond to free AO^+ in water and the AO^+@CB[7] complex, respectively (Table 1), in agreement with previously reported data.[21,44,45]

The initial anisotropy for AO^+ was determined in glycerol to be 0.34 ± 0.01 (inset in Fig. 3). The initial anisotropies recovered from the anisotropy decays of AO^+ in aqueous solution and for the AO^+@CB[7] complex were in the range of 0.30–0.32 (Table 1). These values are close to the glycerol one indicating that no fast rotating component was present for the anisotropy

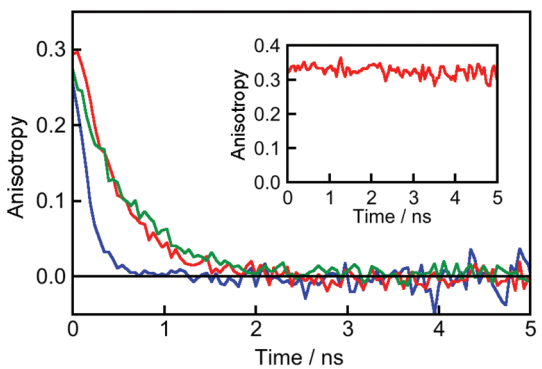

Fig. 3 Fluorescence anisotropy decay for AO^+ (2 μM) in the absence (blue) and presence of 50 μM CB[7] (red) or 20 μM CB[8] (green) in 10 mM phosphate buffer pH 7.0 at 20 °C. Inset: fluorescence anisotropy decay for AO^+ (2 μM) in glycerol at 20 °C.

decay, because in such a case a lower r_0 value would have been obtained. The anisotropy decay for AO^+ in water (Fig. 3) showed a single rotational correlation time of 0.12 ± 0.01 ns, which is in agreement with previously reported values.[46] On the other hand, the anisotropy decay in the presence of CB[7] (Fig. 3) showed a single rotational correlation time of 0.39 ± 0.01 ns. This longer rotational correlation time compared to AO^+ is consistent with the formation of the AO^+@CB[7] complex.

In the presence of CB[8], the fluorescence emission decay was not monoexponential (see Fig. S4 in the ESI†) and two fluorescence lifetimes were recovered. The main component corresponded to a species with a fluorescence lifetime of 6.87 ± 0.02 ns (A_2 = 0.94 ± 0.01). The lifetime of the minor species could not be determined accurately, but it could be fixed to 2.0 ns (A_1 = 0.06 ± 0.01), which is the lifetime of free AO^+ (Table 1). The presence of free AO^+ is possible due to the fact that a large excess of CB[8] cannot be achieved as with CB[7] due to the much lower solubility of CB[8] in water.[1,2] The anisotropy decay in the presence of CB[8] (Fig. 3) showed two rotational correlation times, which could be associated with two fluorescence lifetimes. The rotational correlation time for the species with a lifetime of 2.0 ns could be fixed to 0.12 ns, which is consistent with the presence of AO^+ free in solution. This value was fixed due to the small contribution of this species to the anisotropy decay, which prevented accurate recovery of this parameter.

For the species with a fluorescence lifetime of 6.87 ns, a rotational correlation time of 0.63 ± 0.03 ns was recovered, which is significantly longer than for the AO^+@CB[7] complex (0.39 ± 0.01 ns). When AO^+ was added in a 5-fold excess over CB[8], the same two fluorescence lifetimes were recovered. The latter condition favors the formation of the 2 : 1 complex, suggesting that AO^+ in the 2 : 1 complex has the lifetime of 6.87 ns. Therefore, a rotational correlation time of 0.63 ns was assigned to the rotation of AO^+ in the 2 : 1 complex. The observation of the longer rotational correlation times in the presence of CB[n]s suggests that AO^+ in these complexes does not rotate freely, but rotates with CB[n]s.

It must be noted that an apparent contradiction is inferred between the long fluorescence lifetime and the lower fluorescence intensity observed in the emission spectra of AO^+ in the presence of CB[8] (Fig. 1, inset). The stepwise binding constants and the negative cooperativity found for this system indicate that in the presence of excess CB[8] the main species present is the 1 : 1 complex and this species is poorly fluorescent compared to free AO^+ (Fig. 2). On the other hand, the 2 : 1 complex is a minor species, but with a very long fluorescence lifetime.

The fluorescence lifetime for AO^+ bound to HSA was determined to be 4.77 ± 0.01 ns and this is a minor species in the decay being the major species free AO^+ (Table 1). The anisotropy decay for AO^+ : HSA led to an upward curvature characteristic for the presence of a long rotational correlation time, which was assigned to the formation of the AO^+ : HSA complex (Fig. 4).

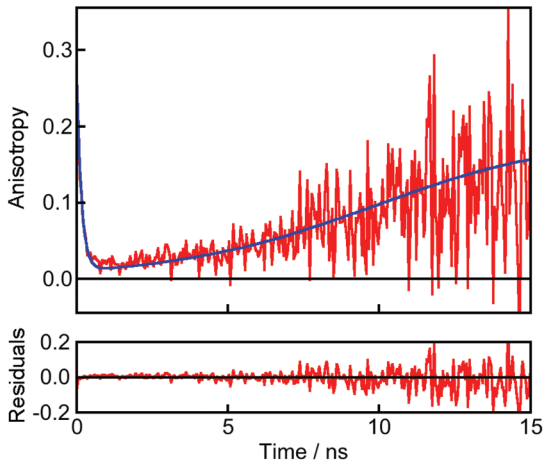

Fig. 4 Fluorescence anisotropy decay for AO^+ (2 μM) in the presence of HSA (10 μM) in 10 mM phosphate buffer pH 7.0 at 20 °C. The data were fit to eqn (4)–(6) in the paper using i = 2 and j = 2.

The rotational correlation time for the AO^+ : HSA complex cannot be determined precisely from this decay because the fluorescence lifetime of AO^+ is too short compared to the rotational correlation time of HSA (39–55 ns).[30] Previously, we reported the rotational correlation time of anthracene carboxylate tightly bound to HSA to be 55 ± 5 ns, since this fluorophore has a high binding constant with HSA and its fluorescence lifetime is longer than AO^+ (1.8–16 ns for different HSA sites).[30] Therefore, in the present work we fixed the long rotational correlation time to 55 ns for the analysis assuming that AO^+ is tightly bound and therefore it rotates with HSA. The recovered rotational correlation time for free AO^+ was 0.15 ± 0.07 ns and the initial anisotropy was 0.30 ± 0.01. The recovered parameters are in good agreement with the values determined in the absence of HSA. The deviations of the fit in the first two nanoseconds could be related to the small presence of loose protein bound species with a shorter rotational correlation time, which cannot be resolved.[30]

3.4. Fluorescence lifetimes and rotational correlation times for the AO^+@CB[7] complex in the presence of HSA

We examined the possible interaction of AO^+@CB[7] with HSA in the presence of an excess CB[7] to ensure quantitative binding of AO^+ to CB[7]. Different ratios for [AO^+@CB[7]]/[HSA] were achieved by changing the concentration of the AO^+@CB[7] complex and keeping the concentration of HSA constant. This procedure avoids introducing scattering or viscosity artifacts in the measurements due to the presence of different concentrations of the protein. The fluorescence lifetime for the AO^+@CB[7] complex showed a slight increase in the presence of HSA at [AO^+@CB[7]]/[HSA] ratios between 0.2 and 5 (Table 2). These differences in the lifetimes are not significant to be assigned to the formation of a new species. However, the anisotropy analysis showed important differences in the rotational correlation times, which suggest the presence of a protein-bound species as shown below.

Table 2 Fluorescence lifetimes and rotational correlation times for different concentrations of AO^+@CB[7] in the presence of 5 μM HSA in 10 mM phosphate buffer pH 7.0 at 20 °C[a]

[AO^+@CB[7]]/[HSA] ratio	τ^b/ns	ϕ_1/ns (β_1)	ϕ_2/ns (β_2)	r_0
0.2	3.47	0.44 ± 0.05 (0.95 ± 0.01)	55^{fixed} (0.05 ± 0.01)	0.33 ± 0.02
1	3.51	0.43 ± 0.04 (0.97 ± 0.01)	55^{fixed} (0.03 ± 0.01)	0.32 ± 0.02
2	3.55	0.43 ± 0.05 (0.98 ± 0.01)	55^{fixed} (0.02 ± 0.01)	0.30 ± 0.02
3	3.65	0.40 ± 0.05 (1)	—	0.32 ± 0.02
4	3.67	0.40 ± 0.05 (1)	—	0.31 ± 0.02
5	3.75	0.41 ± 0.05 (1)	—	0.29 ± 0.02

[a] The ratio between CB[7] and HSA was kept fixed at 10 : 1 to ensure the binding of AO^+ to CB[7] ([CB[7]] = 50 μM; [HSA] = 5 μM). [AO^+] was varied from 1 μM to 25 μM. The errors correspond to the errors of the anisotropy fits. [b] The errors for lifetimes were ≤3%.

The fluorescence anisotropy did not decay to zero within the time-scale of the measurement for [AO^+@CB[7]]/[HSA] ratios between 0.2 (Fig. 5) and 2, but decayed to zero at higher ratios (inset in Fig. 5), indicating the presence of a slow rotating species at lower ratios. These anisotropy decays are very different from the anisotropy decay of the AO^+ : HSA species (Fig. 4), suggesting the presence of a different species. Also, the fluorescence lifetime observed for this system (3.47–3.75 ns) does not agree with the presence of the AO^+ : HSA species.

The anisotropy decays were fit using eqn (4) by assigning two rotational correlation times to the single fluorescence lifetime observed. We observed a short rotational correlation time of 0.44 ± 0.05 ns that was consistent with the rotation of free AO^+@CB[7] complex. The longer rotational correlation time could not be recovered from the fit because its contribution to the anisotropy decay was small (see the ESI† for details). This rotational correlation time could be fixed to the value previously reported for the rotation of a guest bound to HSA (55 ns).[30] The contribution of the longer component to the anisotropy decay decreased at higher [AO^+@CB[7]]/[HSA] ratios (β_2 in Table 2), suggesting that at higher ratios all HSA sites are occupied and the contribution from AO^+@CB[7] in a solution is the predominant species for the decay. Therefore, detection of any interaction with the protein is more evident at low concentration ratios.

The anisotropy analysis indicates the presence of a protein-bound species and it is important to discriminate between the possible formation of a AO^+@CB[7] : HSA complex and the AO^+ : HSA complex, which could be present in small amounts if some displacement of AO^+ occurred from the CB[7] complex into HSA. We performed simulations to further support the assignment of the anisotropy decay shown in Fig. 5 to the formation of a ternary complex instead of displacement into HSA (Fig. S5 in the ESI†). Using the distinctive fluorescence lifetimes and rotational correlation times of each species, we simulated the anisotropy decays under two different scenarios, taking into account the simultaneous presence of AO^+@CB[7] and AO^+ : HSA complexes, or free AO^+@CB[7] and AO^+@CB[7] : HSA complexes (see the ESI† for details). These simulations showed that an upward curvature in the anisotropy decay would have been observed if the AO^+ : HSA complex was the species responsible for the slow rotating component in the anisotropy decay. In contrast, a downward curvature was simulated for the formation of the ternary complex, which is consistent with the experimental data.

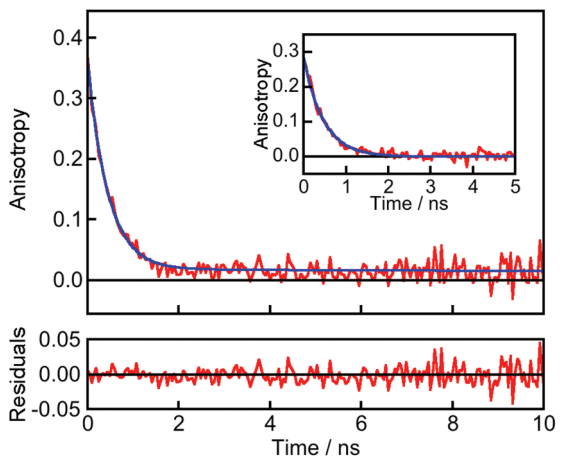

Fig. 5 Fluorescence anisotropy decay for the AO^+@CB[7] complex in the presence of HSA at an [AO^+@CB[7]]/[HSA] ratio of 0.2. Inset: data for an [AO^+@CB[7]]/[HSA] ratio of 5. All samples in 10 mM phosphate buffer pH 7.0 at 20 °C. The data were fit to eqn (4).

3.5. Fluorescence lifetimes and rotational correlation times for the AO^+_2@CB[8] complex in the presence of HSA

Two lifetimes of 2.0 ns and 6.9 ns were observed for AO^+ in the presence of CB[8] and HSA (Table 3). These lifetimes are the same as those determined in the absence of HSA (Table 1), which are assigned to free AO^+ and the AO^+_2@CB[8] complex. It is important to note that the AO^+@CB[8] complex (1 : 1) has a low fluorescence intensity, and therefore, an interaction with HSA could be non-detectable in the anisotropy experiments; thus we focused on the AO^+_2@CB[8] complex only. The fluorescence anisotropy decays in the presence of HSA at different concentration ratios (see Fig. S6 in the ESI†) decayed back to the baseline, which is different from the behavior observed in the presence of CB[7] (compare Fig. S6† with Fig. 5). The decays were analyzed using the associated model by assigning one rotational correlation time to each species (eqn (4)–(6)). A short rotational correlation time that could be fixed to 0.12 ns was associated with the species with a fluorescence lifetime of

Table 3 Fluorescence lifetimes and rotational correlation times for different concentrations of AO^+ in the presence of excess CB[8] and 5 μM HSA in 10 mM phosphate buffer pH 7.0 at 20 °C[a]

$[AO^+]_{total}$/[HSA] ratio	τ_1 [b]/ns (A_1)	τ_2 [b]/ns (A_2)	ϕ_1/ns	ϕ_2/ns	r_0
1	2.0^{fixed} (0.10)	6.94 (0.90)	0.12^{fixed}	0.54 ± 0.03	0.28 ± 0.01
2	2.0^{fixed} (0.05)	6.91 (0.95)	0.12^{fixed}	0.49 ± 0.02	0.30 ± 0.01
3	2.0^{fixed} (0.03)	6.93 (0.97)	0.12^{fixed}	0.52 ± 0.02	0.27 ± 0.01
4	2.0^{fixed} (0.04)	6.91 (0.96)	0.12^{fixed}	0.51 ± 0.02	0.27 ± 0.01

[a] The ratio between CB[8] and HSA was kept fixed at 8 : 1 to ensure the binding of AO^+ to CB[8] ([CB[8]] = 40 μM; [HSA] = 5 μM). $[AO^+]$ was varied from 1 μM to 20 μM. The ratios in the table are based on the total AO^+ concentration rather than the actual concentration of the 2 : 1 complex present in the solutions. The errors correspond to the error of the fits. [b] The errors for lifetimes and A values were ≤3%.

2.0 ns, while a rotational correlation time of 0.54 ± 0.03 ns was recovered for the species with a fluorescence lifetime of 6.94 ns at the lowest concentration ratio used. The same results were observed for samples at higher concentration ratios (Table 3). The rotational correlation times observed in the presence of HSA were slightly shorter than in the absence of HSA, which we attribute to scattering artifacts in the presence of CB[8] (see Fig. S7 in the ESI†). The relevant point here is that the anisotropy decayed to zero at all the ratios studied (see Fig. S6 in the ESI†), indicating the absence of a slow rotating species that could be otherwise attributed to the formation of a complex with HSA. These results suggest that no association between the AO^+_2@CB[8] complex and HSA is present in the system.

3.6. HSA fluorescence quenching in the presence of AO^+@CB-[n] complexes

We corroborated the formation of a ternary complex between AO^+@CB[7] and HSA by using the quenching of the fluorescence emission from the single tryptophan residue in HSA as reported by other authors.[22] The fluorescence intensity of HSA decreased significantly in the presence of increasing concentrations of AO^+@CB[7], indicating the quenching of the singlet excited state of HSA (see Fig. S8 in the ESI†). All AO^+ was bound to CB[7] since a large excess of CB[7] compared to HSA was used. The inner-filter effect arising from AO^+@CB[7] absorption of light at excitation and emission wavelengths was taken into account and the fluorescence intensity was corrected according to a reported procedure.[34,35] We corroborated that the quenching was static since there was no change in the fluorescence lifetimes of HSA in the presence of the AO^+@CB-[7] complex (see Table S1 in the ESI†), indicating that the quencher (AO^+@CB[7]) is located close to the emitting species (HSA tryptophan). This result further supports the formation of a ternary complex. The fluorescence quenching data were analyzed using a Stern–Volmer plot (eqn (1)), where K_{SV} corresponds to a binding constant assuming a 1 : 1 stoichiometry between AO^+@CB[7] and HSA (Fig. 6).[34] The value obtained was $(3.5 \pm 0.8) \times 10^4$ M^{-1}. This binding constant is not significantly different from $(2.5 \pm 0.4) \times 10^4$ M^{-1} obtained for the binding between AO^+ and HSA in the absence of CB[7] (see above). It is important to remark that fluorescence quenching analysis does not allow to differentiate between the AO^+ : HSA and the AO^+@CB[7] : HSA complexes, as opposed to time-resolved anisotropy measurements. Finally, little quenching of the HSA emission was observed in the presence of AO^+ and CB[8] (I_0/I lower than 1.06), which agrees with the fact that no interaction was observed for the CB[8] complex using fluorescence anisotropy measurements.

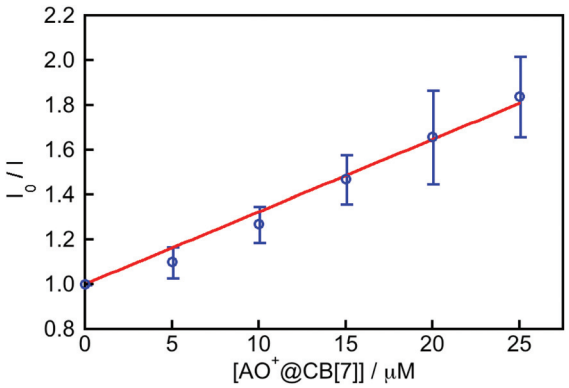

Fig. 6 Stern–Volmer plot for HSA (5 μM) quenched with AO^+@CB[7] complex in 10 mM phosphate buffer pH 7.0 at 20 °C.

4. Discussion

The study of the supramolecular interactions between drug@CB[n] complexes and proteins is of potential interest when examining the behavior of CB[n] as drug carriers in biological systems.[9,10,12,15–17] In this context, the results shown in this work suggest that a combination of fluorescence lifetime determination, quenching studies and time-resolved fluorescence anisotropy measurements provides a powerful tool to study supramolecular interactions in such complex systems. It is important to highlight the sensibility of the analysis proposed here, since the protein-bound species were minor but different enough to distinguish them from each other.

The first important analysis in this work was the determination of the binding constants for AO^+@CB[n] and AO^+ : HSA complexes. AO^+ showed higher binding affinities for CB[n] compared to HSA, and therefore, displacement into HSA did not occur significantly. AO^+ binds with a 1 : 1 stoichiometry to CB[7] and the analysis of the binding isotherm is straightforward. On the other hand, determination of binding constants to CB[8] is difficult due to the possibility of including

one or two molecules inside this macrocycle, which has limited the number of stepwise binding constants reported in the literature.[28] Recently, the stepwise binding of berberine to CB[8] and the kinetics for the process were determined using fluorescence measurements.[28] We report here a simple approach to determine the stepwise binding constants for AO^+ with CB[8] based on numerical analysis of the fluorescence data, which should be broadly applicable to other fluorescent guests. We tested the analysis by determining stepwise binding constants for a known system and the results were comparable to those reported with other techniques. Moreover, the overall binding of the two AO^+ molecules to CB[8], which had been recognized before in the literature,[15,20] agreed well with the overall binding constant determined here, further validating our method. Stepwise binding constants for CB[8] complexes were essential for the assignment of the fluorescence lifetimes and rotational correlation times (see below), since they provided information on the relative concentrations of different species.

The photophysical characterization of different species was clear for free AO^+, AO^+@CB[7] complex and AO^+ : HSA complex. On the other hand, AO^+ and CB[8] form complexes with 1 : 1 and 2 : 1 stoichiometries and the assignment was not straightforward. The very low fluorescence intensity for AO^+ in the presence of CB[8] observed here and by others[15,20] seems to contradict the long fluorescence lifetime observed for this system. Although previous reports have rationalized the lower emission quantum yield of AO^+ in the presence of CB[8] as self-quenching due to π–π stacking in the 2 : 1 complex,[15,20] the stepwise binding constants and the negative cooperativity we found for this system indicate that it is the 1 : 1 complex that is poorly fluorescent. It has been recently suggested that the presence of water molecules inside the cavity quench the emission of a single berberine molecule included inside CB[8].[27,28] We propose then that the reason behind the quenching of the AO^+ fluorescence in the 1 : 1 complex is the presence of high-energy water molecules inside the cavity of CB[8],[47] and not self-quenching. Recent theoretical and experimental fluorescence studies comparing the gas phase to solution show that AO^+ exposure to water molecules decreases the fluorescence quantum yield and shortens the lifetime for excited AO^+.[48] All these data are consistent with water quenching of AO^+ fluorescence inside CB[8] for the 1 : 1 complex. On the other hand, the assignment of the 2 : 1 complex to the species with a fluorescence lifetime of 6.9 ns is consistent with the fact that the lifetime for the AO^+ dimer in water is longer than that for the monomer (8–9 ns).[44,45]

Time-resolved anisotropy measurements were essential to differentiate between free AO^+ and/or CB[*n*] complexed species from HSA-bound species because the changes in the fluorescence lifetimes were not sufficiently significant to identify the presence of the minor species, that is the ternary complex. It must be pointed out that the changes in the anisotropy decays were small, but noticeable. The importance of combining lifetime measurements with the determination of rotational correlation times and simulations of the anisotropy decays came to the forefront in this study because it enabled the differentiation between the different types of complexes formed. In this context, it is important to perform experiments at different concentration ratios to maximize the ability to detect minor species. These types of studies will make possible the detection of new supramolecular interactions with the protein. The relevance of the anisotropy experiments is highlighted by the fact that the traditional quenching experiments used to differentiate between free and protein bound species,[34] were not useful in the current study since the quenching efficiencies of the HSA emission by AO^+ and AO^+@CB[7] were the same.

It is interesting to note that only the AO^+@CB[7] complex seems to interact with the protein and not the AO^+_2@CB[8] complex, based on the combined fluorescence analysis presented here. ^{1}H NMR studies,[49,50] and computer calculations,[48] show that protonation of the central nitrogen of AO^+ induces a configuration in the complex where AO^+ protrudes from the CB[7] cavity.[48] The fact that AO^+ is only partially encapsulated into CB[7] possibly allows the interaction of the protruding moiety of AO^+ with HSA, and/or makes possible the interaction of a protein amino acid with the partially filled CB[7] cavity. This particular protrusion feature of the complexes has been previously observed in protein ternary complexes.[22,29] There is no information available on the structure for the complexes of AO^+ with CB[8]. However, one possibility is that the larger size of CB[8] can fully seclude AO^+ without generating a protruding moiety to interact with HSA.

5. Conclusions

The present work highlights the usability of a combined fluorescence lifetime and anisotropy approach as a tool to study supramolecular interactions in ternary systems composed of a guest, CB[*n*]s and proteins. High binding affinities of guests to CB[*n*]s are needed in order to ensure that no relocation of the guest into the protein occurs, thus favoring ternary supramolecular interactions in the case of CB[7] but not CB[8]. The analysis used in this work also uncovered that in the stepwise formation of the 1 : 1 and 2 : 1 AO^+ complexes with CB[8], which shows negative cooperativity, the 1 : 1 complex is weakly fluorescent while the 2 : 1 complex is the fluorescent species.

Acknowledgements

The authors thank CONICYT for the financial support through their FONDECYT research program (Grant no. 11121223) and the Pontificia Universidad Catolica de Chile through VRA for the partial financing of a research stay at the University of Victoria. The research at the University of Victoria was supported by a Discovery Grant from the Natural Sciences and Engineering Council of Canada (NSERC) to CB.

Notes and references

1 J. Kim, I.-S. Jung, S.-Y. Kim, E. Lee, J.-K. Kang, S. Sakamoto, K. Yamaguchi and K. Kim, New Cucurbituril Homologues: Syntheses, Isolation, Characterization, and X-ray Crystal Structures of Cucurbit[n]uril (n = 5, 7, and 8), *J. Am. Chem. Soc.*, 2000, **122**, 540–541.

2 J. Lagona, P. Mukhopadhyay, S. Chakrabarti and L. Isaacs, The cucurbit[n]uril family, *Angew. Chem., Int. Ed.*, 2005, **44**, 4844–4870.

3 Y. H. Ko, I. Hwang, D.-W. Lee and K. Kim, Ultrastable Host-guest Complexes and their Applications, *Isr. J. Chem.*, 2011, **51**, 506–514.

4 A. R. Urbach and V. Ramalingam, Molecular Recognition of Amino Acids, Peptides, and Proteins by Cucurbit[n]uril Receptors, *Isr. J. Chem.*, 2011, **51**, 664–678.

5 F. Biedermann and W. M. Nau, Noncovalent Chirality Sensing Ensembles for the Detection and Reaction Monitoring of Amino Acids, Peptides, Proteins, and Aromatic Drugs, *Angew. Chem., Int. Ed.*, 2014, **53**, 5694–5699.

6 Y. Ahn, Y. Jang, N. Selvapalam, G. Yun and K. Kim, Supramolecular Velcro for Reversible Underwater Adhesion, *Angew. Chem., Int. Ed.*, 2013, **125**, 3222–3226.

7 Y. Lan, Y. Wu, A. Karas and O. A. Scherman, Photoresponsive Hybrid Raspberry-Like Colloids Based on Cucurbit[8]-uril Host–Guest Interactions, *Angew. Chem., Int. Ed.*, 2014, **53**, 2166–2169.

8 H. Jung, J. S. Park, J. Yeom, N. Selvapalam, K. M. Park, K. Oh, J.-A. Yang, K. H. Park, S. K. Hahn and K. Kim, 3D Tissue Engineered Supramolecular Hydrogels for Controlled Chondrogenesis of Human Mesenchymal Stem Cells, *Biomacromolecules*, 2014, **15**, 707–714.

9 K. M. Park, K. Suh, H. Jung, D.-W. Lee, Y. Ahn, J. Kim, K. Baek and K. Kim, Cucurbituril-based Nanoparticles: A New Efficient Vehicle for Targeted Intracellular Delivery of Hydrophobic Drugs, *Chem. Commun.*, 2009, 71–73.

10 C. Kim, S. S. Agasti, Z. Zhu, L. Isaacs and V. M. Rotello, Recognition-Mediated Activation of Therapeutic Gold Nanoparticles Inside Living Cells, *Nat. Chem.*, 2010, **2**, 962–966.

11 D. H. Macartney, Encapsulation of Drug Molecules by Cucurbiturils:Effects on their Chemical Properties in Aqueous Solution, *Isr. J. Chem.*, 2011, **51**, 600–615.

12 S. Walker, R. Oun, F. J. McInees and N. J. Wheate, The Potential of Cucurbit[n]urils in Drug Delivery, *Isr. J. Chem.*, 2011, **51**, 616–624.

13 F. Biedermann, V. D. Uzunova, O. A. Scherman, W. M. Nau and A. De Simone, Release of High-Energy Water as an Essential Driving Force for the High-Affinity Binding of Cucurbit[n]urils, *J. Am. Chem. Soc.*, 2012, **134**, 15318–15323.

14 H.-J. Schneider, *Supramolecular Systems in Biomedical Fields*, Royal Society of Chemistry, 2013.

15 P. Montes-Navajas, M. Gonzalez-Bejar, J. C. Scaiano and H. Garcıa, Cucurbituril Complexes Cross The Cell Membrane, *Photochem. Photobiol. Sci.*, 2009, **8**, 1743–1747.

16 G. Hettiarachchi, D. Nguyen, J. Wu, D. Lucas, D. Ma, L. Isaacs and V. Briken, Toxicology and Drug Delivery by Cucurbit[n]uril Type Molecular Containers, *PLoS One*, 2010, **5**, 10514.

17 V. D. Uzunova, C. Cullinane, K. Brix, W. M. Nau and A. I. Day, Toxicity of Cucurbit[7]uril and Cucurbit[8]uril: An Exploratory In Vitro and In Vivo Study, *Org. Biomol. Chem.*, 2010, **8**, 2037–2042.

18 S. Monti and I. Manet, Supramolecular Photochemistry of Drugs in Biomolecular Environments, *Chem. Soc. Rev.*, 2014, **43**, 4051–4067.

19 I. Vayá, V. Lhiaubet-Vallet, M. C. Jiménez and M. A. Miranda, Photoactive Assemblies of Organic Compounds and Biomolecules: Drug–Protein Supramolecular Systems, *Chem. Soc. Rev.*, 2014, **43**, 4102–4122.

20 P. Montes-Navajas, A. Corma and H. Garcia, Complexation and Fluorescence of Tricyclic Basic Dyes Encapsulated in Cucurbiturils, *ChemPhysChem*, 2008, **9**, 713–720.

21 M. Shaikh, J. Mohanty, P. K. Singh, W. M. Nau and H. Pal, Complexation of Acridine Orange by Cucurbit[7]uril and beta-Cyclodextrin: Photophysical Effects and pKa Shifts, *Photochem. Photobiol. Sci.*, 2008, **7**, 408–414.

22 W. Lei, G. Jiang, Q. Zhou, B. Zhang and X. Wang, Greatly Enhanced Binding of a Cationic Porphyrin Towards Bovine Serum Albumin by Cucurbit[8]uril, *Phys. Chem. Chem. Phys.*, 2010, **12**, 13255–13260.

23 C. Bohne, Supramolecular Dynamics, *Chem. Soc. Rev.*, 2014, **43**, 4037–4050.

24 C. Marquez and W. M. Nau, Two Mechanisms of Slow Host–Guest Complexation between Cucurbit[6]uril and Cyclohexylmethylamine: pH-Responsive Supramolecular Kinetics, *Angew. Chem., Int. Ed.*, 2001, **40**, 3155–3160.

25 C. Márquez, R. R. Hudgins and W. M. Nau, Mechanism of Host-Guest Complexation by Cucurbituril, *J. Am. Chem. Soc.*, 2004, **126**, 5806–5816.

26 H. Tang, D. Fuentealba, Y. H. Ko, N. Selvapalam, K. Kim and C. Bohne, Guest Binding Dynamics with Cucurbit[7]-uril in the Presence of Cations, *J. Am. Chem. Soc.*, 2011, **133**, 20623–20633.

27 Z. Miskolczy and L. Biczók, Kinetics and Thermodynamics of Berberine Inclusion in Cucurbit[7]uril, *J. Phys. Chem. B*, 2014, **118**, 2499–2505.

28 Z. Miskolczy and L. Biczók, Sequential Inclusion of Two Berberine Cations in Cucurbit[8]uril Cavity: Kinetic and Thermodynamic Studies, *Phys. Chem. Chem. Phys.*, 2014, **16**, 20147–20156.

29 A. C. Bhasikuttan, J. Mohanty, W. M. Nau and H. Pal, Efficient Fluorescence Enhancement and Cooperative Binding of an Organic Dye in a Supra-biomolecular Host–Protein Assembly, *Angew. Chem., Int. Ed.*, 2007, **119**, 4198–4200.

30 D. Fuentealba, H. Kato, M. Nishijima, G. Fukuhara, T. Mori, Y. Inoue and C. Bohne, Explaining the Highly Enantiomeric Photocyclodimerization of 2-Anthracenecarboxylate Bound to Human Serum Albumin Using Time-Resolved Anisotropy Studies, *J. Am. Chem. Soc.*, 2013, **135**, 203–209.

31 X.-Z. Feng, Z. Lin, L.-J. Yang, C. Wang and C.-L. Bai, Investigation of the Interaction Between Acridine Orange and Bovine Serum Albumin, *Talanta*, 1998, **47**, 1223–1229.
32 E. Vogelmann, W. Rauscher and H. E. A. Kramer, Reactivity of Acridine Dye Triplet States in Electron Transfer Reactions, *Photochem. Photobiol.*, 1979, **29**, 771–776.
33 S. Yi and A. E. Kaifer, Determination of the Purity of Cucurbit[n]uril (n = 7, 8) Host Samples, *J. Org. Chem.*, 2011, **76**, 10275–10278.
34 J. R. Lakowicz, *Principles of Fluorescence Spectroscopy*, Springer, New York, 4th edn, 2006.
35 R. A. Leese and E. L. Wehry, Corrections for Inner-Filter Effects in Fluorescence Quenching Measurements *via* Right-Angle and Front-Surface Illumination, *Anal. Chem.*, 1978, **50**, 1193–1197.
36 C. Bohne, R. W. Redmond and J. C. Scaiano, Use of Photophysical Techniques in the Study of Organized Assemblies, in *Photochemistry in Organized and Constrained Media*, ed. V. Ramamurthy, VCH Publishers, New York, 1991, pp. 79–132.
37 R. D. Ludescher, L. Peting, S. Hudson and B. Hudson, Time-Resolved Fluorescence Anisotropy For Systems with Lifetime and Dynamic Heterogeneity, *Biophys. Chem.*, 1987, **28**, 59–75.
38 W. L. F. Armarego and C. L. L. Chai, *Purification of Laboratory Chemicals*, Elsevier, Burlington, 6th edn, 2009.
39 B. H. Robinson, A. Löffler and G. Schwarz, Thermodynamic Behaviour of Acridine Orange in Solution. Model System for studying Stacking and Charge-effects on Self-aggregation, *J. Chem. Soc., Faraday Trans. 1*, 1973, **69**, 56–69.
40 K. A. Connors, *Binding Constants. The Measure of Molecular Complex Stability*, John Wiley & Sons, Inc., New York, 1987.
41 L. M. Heitmann, A. B. Taylor, P. J. Hart and A. R. Urbach, Sequence-Specific Recognition and Cooperative Dimerization of N-Terminal Aromatic Peptides in Aqueous Solution by a Synthetic Host, *J. Am. Chem. Soc.*, 2006, **128**, 12574–12581.
42 G. Sudlow, D. J. Birkett and D. N. Wade, The Characterization of Two Specific Drug Binding Sites on Human Serum Albumin, *Mol. Pharmacol.*, 1975, **11**, 824–832.
43 M. Shaikh, S. D. Choudhury, J. Mohanty, A. C. Bhasikuttan and H. Pal, Contrasting Guest Binding Interaction of Cucurbit[7–8]urils with Neutral Red Dye: Controlled Exchange of Multiple Guests, *Phys. Chem. Chem. Phys.*, 2010, **12**, 7050–7055.
44 N. Miyoshi, K. Hara, I. Yokoyama, G. Tomita and M. Fukuda, Fluorescence Lifetime of Acridine Orange in Sodium Dodecyl Sulfate Premicellar Solutions, *Photochem. Photobiol.*, 1988, **47**, 685–688.
45 R. D. Falcone, N. M. Correa, M. A. Biasutti and J. J. Silber, Acid–Base and Aggregation Processes of Acridine Orange Base in n-Heptane/AOT/Water Reverse Micelles, *Langmuir*, 2002, **18**, 2039–2047.
46 A. K. Shaw and S. K. Pal, Fluorescence Relaxation Dynamics of Acridine Orange in Nanosized Micellar Systems and DNA, *J. Phys. Chem. B*, 2007, **111**, 4189–4199.
47 F. Biedermann, M. Vendruscolo, O. A. Scherman, A. De Simone and W. M. Nau, Cucurbit[8]uril and Blue-Box: High-Energy Water Release Overwhelms Electrostatic Interactions, *J. Am. Chem. Soc.*, 2013, 135.
48 M. F. Czar and R. A. Jockusch, Understanding Photophysical Effects of Cucurbituril Encapsulation: A Model Study with Acridine Orange in the Gas Phase, *ChemPhysChem*, 2013, **14**, 1138–1148.
49 S.-H. Chou and M. J. Wirth, Rotational Diffusion of Acridine Orange Attached to SDS Mlcelles, *J. Phys. Chem.*, 1989, **93**, 7694–7698.
50 J. Liu, N. Jiang, J. Ma and X. Du, Insight into Unusual Downfield NMR Shifts in the Inclusion Complex of Acridine Orange with Cucurbit[7]uril, *Eur. J. Org. Chem.*, 2009, 4931–4938.